Published for SISSA by Springer

Received: *September 20, 2013*
Revised: *December 3, 2013*
Accepted: *December 11, 2013*
Published: *December 23, 2013*

NLO corrections to WWZ production at the LHC

DAO Thi Nhung,[a,b] **LE Duc Ninh**[a,b,1] **and Marcus M. WEBER**[c]

[a] *Institut für Theoretische Physik, Karlsruher Institut für Technologie, D-76128 Karlsruhe, Germany*

[b] *Institute of Physics, Vietnam Academy of Science and Technology, 10 Dao Tan, Ba Dinh, Hanoi, Vietnam*

[c] *Max-Planck-Institut für Physik (Werner-Heisenberg-Institut), D-80805 München, Germany*

E-mail: thi.dao@kit.edu, duc.le@kit.edu, mmweber@mppmu.mpg.de

Abstract: The production of W^+W^-Z at the LHC is an important process to test the quartic gauge couplings of the Standard Model as well as an important background for new physics searches. A good theoretical understanding at next-to-leading order (NLO) is therefore valuable. In this paper, we present the calculation of the NLO electroweak (EW) correction to this channel with on-shell gauge bosons in the final state. It is then combined with the NLO QCD correction to get the most up-to-date prediction. We study the impact of these corrections on the total cross section and some distributions. The NLO EW correction is small for the total cross section but becomes important in the high energy regime for the gauge boson transverse momentum distributions.

Keywords: NLO Computations, Hadronic Colliders

ArXiv ePrint: 1307.7403

[1] Corresponding author.

doi:10.1007/JHEP12(2013)096

JHEP12(2013)096

Contents

JHEP12(2013)096

1 Introduction

The program to check the Standard Model (SM) is on good course with the recent discovery of a new boson with a mass of about 125 GeV at the ATLAS [1] and CMS [2] experiments. The present data seem to indicate that this new particle is consistent with the long-sought SM Higgs boson, whose existence is a prediction of the SM. Once the particle list is confirmed and their masses are measured, we have to make sure that all the SM couplings are consistent with the data. In this project, we have to check the quartic couplings of gauge bosons, which are renormalizable and occur in the SM Lagrangian as a consequence of non-Abelian gauge symmetry.

If we take a proton-proton collider and ask the question what is a good process to test the quartic couplings W^+W^-ZZ and $W^+W^-Z\gamma$ then we find that there are two mechanisms at tree level. The four-point vertex is attached to either one quark line or two quark lines. In this paper we consider the former with three massive gauge bosons in the final state, namely the process $pp \to W^+W^-Z$. In addition, this process is an important background for new physics searches.

The tree-level requirement is important to have high sensitivity to the couplings. In order to compare the SM prediction with experimental data, the tree-level calculation is, however, not good enough since it suffers from large theoretical uncertainties. A full next-to-leading-order (NLO) calculation including both QCD and EW corrections is needed to reduce the uncertainty and to understand the quantum-loop effects. The NLO QCD corrections have been calculated by two groups: in ref. [3] including leptonic decays of the gauge bosons and in ref. [4] in the heavy Higgs limit. In this paper we recalculate the QCD

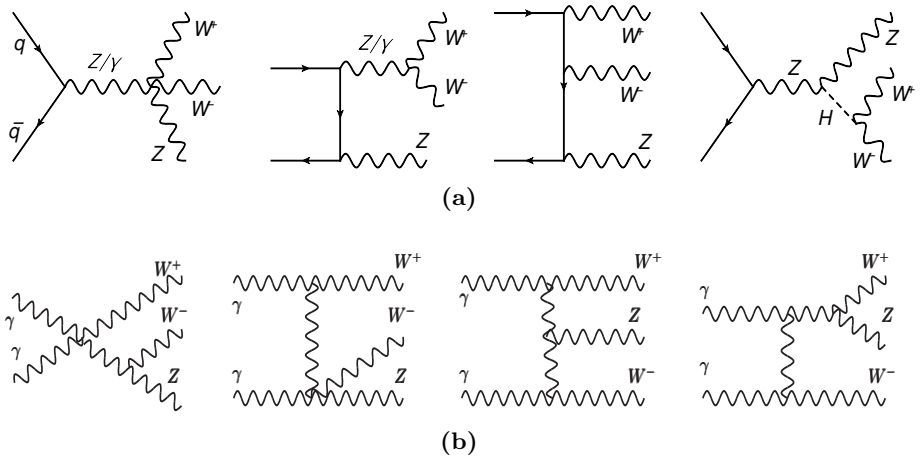

Figure 1. Representative tree-level diagrams for the $q\bar{q} \to W^+W^-Z$ subprocesses (a) and the $\gamma\gamma \to W^+W^-Z$ subprocess (b).

corrections and, for the first time, the full NLO EW corrections to the on-shell W^+W^-Z production at the large hadron collider (LHC) are calculated.

The paper is organized as follows. The calculation of NLO QCD and EW corrections is discussed in section 2. The definition of hadronic cross section is also given there. In section 3, numerical results for the total cross section and some representative distributions are presented. We discuss also the use of jet veto to reduce large QCD correction. Conclusions are found in the last section. In the appendix we provide results at the amplitude squared level at a random phase-space point to facilitate comparisons with our results.

2 Calculational details

The tree-level subprocesses are

$$\bar{q} + q \to W^+ + W^- + Z, \tag{2.1}$$

$$\bar{b} + b \to W^+ + W^- + Z, \tag{2.2}$$

$$\gamma + \gamma \to W^+ + W^- + Z, \tag{2.3}$$

where q stands for the light quarks (u, d, c, s) if not otherwise stated. The $q\bar{q}$ contributions are dominant and their Feynman diagrams can be divided into four distinct topologies as depicted in figure 1a. It should be noted that the s-channel diagrams with an intermediate Higgs boson are included in our calculation. The Higgs contribution including interference effects is less than 1% at leading order (LO) for $M_H = 125\,\text{GeV}$. Since the bottom-quark and photon distribution functions are much smaller than those of the light quarks, the $b\bar{b}$ and $\gamma\gamma$ contributions are much less important. We therefore include them only at LO. In figure 1b, a representative set of tree-level diagrams for $\gamma\gamma \to W^+W^-Z$ is presented.

In the following we discuss the NLO QCD and EW corrections to the subprocesses (2.1). We will define the various sub-corrections at NLO, namely the QCD virtual, gluon-radiated and gluon-quark induced corrections for the QCD case and the EW virtual, photon-radiated

JHEP12(2013)096

and photon-quark induced corrections for the EW case. These sub-corrections are ultraviolet (UV) and infrared (IR) finite, but are dependent on the regularization scheme. The final results, i.e. the sum of those sub-corrections, are regularization-scheme independent. The separation will provide more insights into the QCD and EW corrections.

2.1 NLO QCD corrections

The NLO QCD contribution contains the virtual and real-emission corrections. The virtual Feynman diagrams with an extra gluon in the loops include pentagon diagrams up to rank four. The one-loop tensor integrals are calculated using Passarino-Veltman reduction [5] for up to four-point diagrams and the method of ref. [6] (see also ref. [7]) for five-point tensor integrals. The scalar integrals are calculated as in refs. [8–11]. The UV divergences of the loop integrals are regularized using dimensional regularization (DR) [12]. Since the light quarks are approximated as massless, their mass counterterms vanish.

The real-emission processes are classified into the gluon-radiated processes

$$\bar{q} + q \to W^+ + W^- + Z + g \tag{2.4}$$

and the gluon-quark induced processes

$$\begin{aligned} q + g &\to W^+ + W^- + Z + q, \\ \bar{q} + g &\to W^+ + W^- + Z + \bar{q}. \end{aligned} \tag{2.5}$$

Both the virtual and real corrections are separately IR divergent. These divergences cancel in the sum for infrared-safe observables such as the total cross section and kinematic distributions of massive gauge bosons. The IR singularities are treated using the DR and mass regularization (MR) schemes (see also section 2.3). MR method uses a common mass regulator for the light fermions (all but the top quark) and a fictitious gluon mass. The results of two schemes are in agreement.

Moreover, we apply the Catani-Seymour dipole subtraction algorithm [13] to combine the virtual and the real contributions. We use the same notations as in ref. [13] with the DR method and define the various NLO QCD corrections as follows,

$$\begin{aligned} \sigma_{\text{QCD-virt}} &= \int \mathrm{d}x_1 \mathrm{d}x_2 [\bar{q}_{\text{NLO}}(x_1,\mu_F) q_{\text{NLO}}(x_2,\mu_F) \hat{\sigma}^{\bar{q}q\to W^+W^-Z}_{\text{QCD-virt}} + (1 \leftrightarrow 2)], \\ \hat{\sigma}^{\bar{q}q\to W^+W^-Z}_{\text{QCD-virt}} &= \hat{\sigma}^{\bar{q}q\to W^+W^-Z}_{\text{QCD-loop}} + \hat{\sigma}^{\bar{q}q\to W^+W^-Z}_{\text{QCD-I}}, \end{aligned} \tag{2.6}$$

where $\hat{\sigma}^{\bar{q}q\to W^+W^-Z}_{\text{QCD-loop}}$ includes only loop diagrams and $\hat{\sigma}^{\bar{q}q\to W^+W^-Z}_{\text{QCD-I}}$ is the I-operator contribution as defined in ref. [13]. It is noted that $\hat{\sigma}^{\bar{q}q\to W^+W^-Z}_{\text{QCD-virt}}$ is UV and IR finite. The gluon-radiated and gluon-quark induced contributions read

$$\begin{aligned} \sigma_{\text{g-rad}} &= \int \mathrm{d}x_1 \mathrm{d}x_2 [\bar{q}_{\text{NLO}}(x_1,\mu_F) q_{\text{NLO}}(x_2,\mu_F) \left(\hat{\sigma}^{\bar{q}q\to W^+W^-Zg} - \hat{\sigma}^{\bar{q}q\to W^+W^-Z}_{\text{QCD-I}} \right) + (1 \leftrightarrow 2)], \\ \sigma_{\text{g-ind}} &= \int \mathrm{d}x_1 \mathrm{d}x_2 [q_{\text{NLO}}(x_1,\mu_F) g_{\text{NLO}}(x_2,\mu_F) \hat{\sigma}^{qg\to W^+W^-Zq} + (1 \leftrightarrow 2)]. \end{aligned} \tag{2.7}$$

These contributions are also IR finite because the collinear divergences occurring at partonic level are absorbed into the quark PDFs.

JHEP12(2013)096

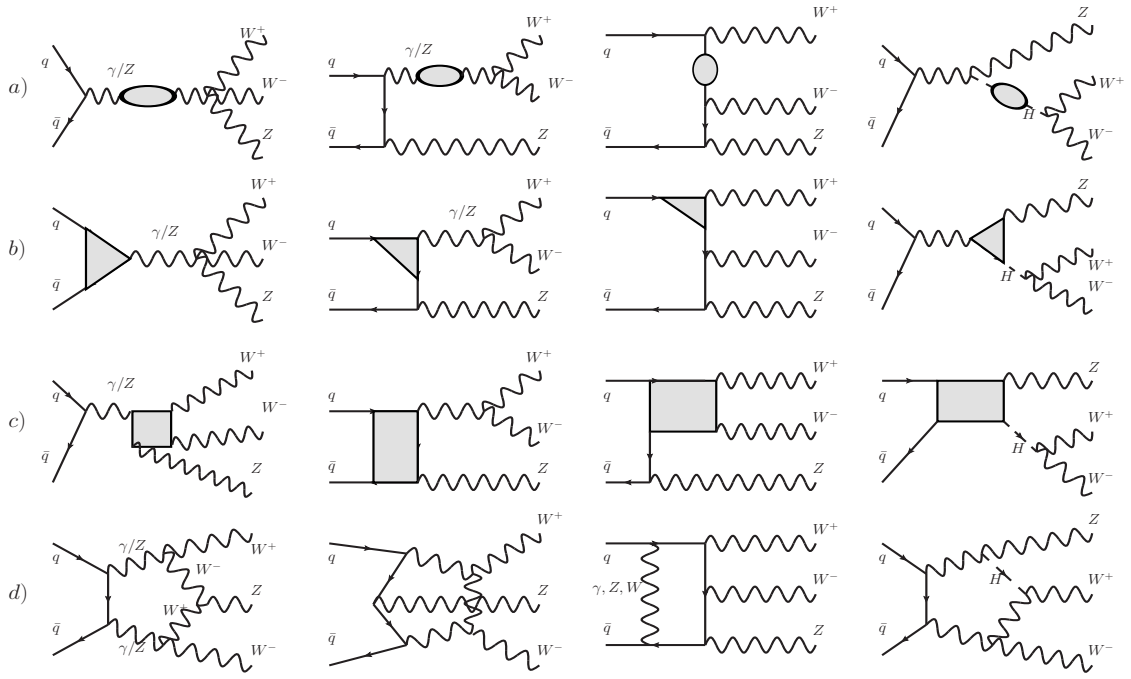

Figure 2. Representative sets of self-energy, vertex, box and pentagon diagrams. The shaded regions are the one-particle irreducible two-, three- and four-point vertices including possible counterterms.

2.2 NLO EW corrections

The NLO EW contribution also includes the virtual and real corrections. Compared to the QCD case, the virtual EW contribution is much more complicated. The one-loop Feynman diagrams contain extra bosons (γ, Z, $W^{\pm}$ or H) in the loops or a fermion loop. The presence of fermion loops with γ_5 requires that all leptons and quarks contribution must be included to cancel the anomaly. For illustration, representative sets of two-, three-, four- and five-point vertices are shown in figure 2(a, b, c, d), respectively. As in the QCD case, the NLO EW corrections involve also five-point tensor integrals up to rank four, see the third Feynman graph in figure 2(d). The one-loop integrals are calculated using the same method as in the QCD case.

We now discuss the issue of renormalization to deal with UV divergences. Renormalization of the electric coupling, the gauge boson masses, the Higgs mass and the external wave functions are performed. We adopt the on-shell renormalization scheme (see refs. [14–16]) where $\alpha(q^2)$ is defined in the Thomson limit at $q^2 \to 0$. However, using $\alpha(0)$ as an input parameter induces large corrections of the form $\log(Q^2/m_f^2)$ with Q being a typical hard energy scale and m_f the light fermion masses in the loop contribution. Those corrections can be absorbed into the running of α using $\alpha(M_Z^2)$ or using the G_μ-scheme with $\alpha_{G_\mu} = \sqrt{2} G_\mu M_W^2 (1 - M_W^2/M_Z^2)/\pi$ as an input parameter (see refs. [17–19]). We choose the latter and hence the calculation is consistently done by fixing the renormalization constant

JHEP12(2013)096

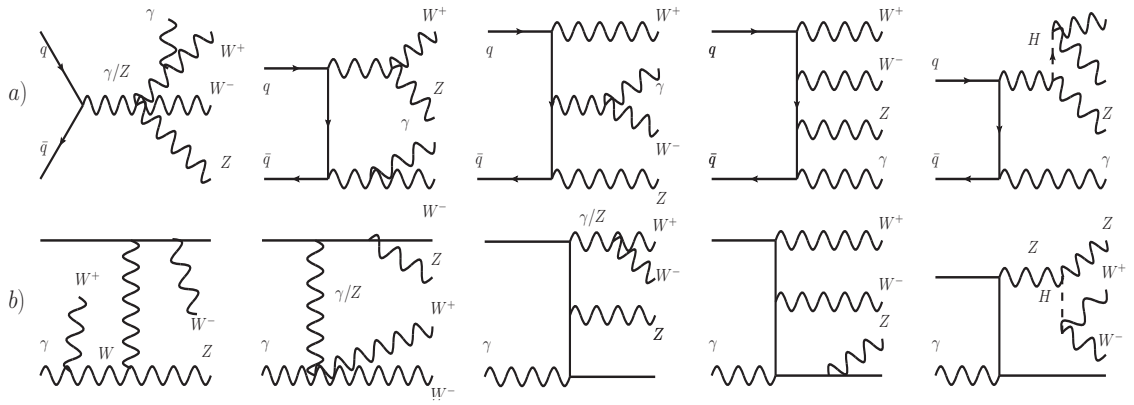

Figure 3. Representative Feynman diagrams for the real photon radiation a) and the photon-quark induced subprocesses b). The solid straight lines stand for the (anti-)quarks.

of the electric charge as

$$\delta Z_e^{G_\mu} = \delta Z_e^{\alpha(0)} - \frac{1}{2}(\Delta r)_{\text{1-loop}}, \tag{2.8}$$

where $(\Delta r)_{\text{1-loop}}$ is defined in refs. [15, 17]. An advantage of this framework is that the final results are independent of the light fermion masses. For vertices with a real photon directly attached to them, the most natural choice is using the coupling $\alpha(0)$. This fixes the NLO EW corrections to $\bar{q}q \to WWZ$ processes proportional to $\alpha^3_{G_\mu}\alpha(0)$. We note that this input-parameter scheme has been used in previous NLO EW calculations, see e.g. ref. [20].

The real-emission corrections contain an extra photon in the external state. Similar to the QCD case, we have the photon-radiated processes

$$\bar{q} + q \to W^+ + W^- + Z + \gamma \tag{2.9}$$

and the photon-quark induced processes

$$\begin{aligned} q + \gamma &\to W^+ + W^- + Z + q, \\ \bar{q} + \gamma &\to W^+ + W^- + Z + \bar{q}, \end{aligned} \tag{2.10}$$

whose Feynman diagrams are shown in figure 3(a,b), respectively. Compared to the real-gluon emission correction, the IR-singularity structure in the photonic correction is much more complicated. In the real-photon radiation case, the singularities arise from two types of splittings: $q \to q^*\gamma$ and $W^* \to W\gamma$. The former gives rise to both soft and collinear divergences while the latter introduces only soft divergences. For the photon-quark induced subprocesses, there occur only collinear divergences arising from the following splittings: $q \to q\gamma^*$ and $\gamma \to q^*\bar{q}$.

In order to deal with those IR divergences and to combine the real-emission and virtual corrections, we will follow the convention of ref. [21]. We use the MR method to regularize IR divergences. For the $\bar{q}q \to W^+W^-Z$ processes, the correction $\sigma_{\text{EW-virt}}$ is, similarly to

JHEP12(2013)096

the QCD case, given as in eq. (2.6), but the I-operator contribution $\hat{\sigma}^{\bar{q}q\to W^+W^-Z}_{\text{EW-I}}$ is now defined as the endpoint contribution of ref. [21]. The photon-radiated and photon-quark induced contributions read

$$\sigma_{\gamma\text{-rad}} = \int \mathrm{d}x_1\mathrm{d}x_2[\bar{q}_{\text{NLO}}(x_1,\mu_F)q_{\text{NLO}}(x_2,\mu_F)\left(\hat{\sigma}^{\bar{q}q\to W^+W^-Z\gamma} - \hat{\sigma}^{\bar{q}q\to W^+W^-Z}_{\text{EW-I}}\right) + (1\leftrightarrow 2)],$$
$$\sigma_{\gamma\text{-ind}} = \int \mathrm{d}x_1\mathrm{d}x_2[q_{\text{NLO}}(x_1,\mu_F)\gamma_{\text{NLO}}(x_2,\mu_F)\hat{\sigma}^{q\gamma\to W^+W^-Zq} + (1\leftrightarrow 2)]. \tag{2.11}$$

Since there is at the present no PDF set with NLO EW corrections, we will use in the numerical analysis the LO PDFs everywhere for EW corrections. Moreover, the collinear divergences occurring at the partonic level in the photon-radiated and photon-quark induced contributions are absorbed into the (anti-)quark and photon PDFs using the DIS factorization scheme as described in section 2.3.

To allow better verification of the results the aforementioned method has been implemented in two independent computer codes, using the `FORTRAN 77` and `C++` programming languages. The helicity amplitudes are generated using `FeynArts-3.4` [22] and `FormCalc-6.0` [23] as well as `HELAS` [24, 25]. The scalar and tensor one-loop integrals in one code are evaluated with the `FORTRAN 77` in-house library `LoopInts` while the other program uses another in-house library written in `C++`. Both libraries have an option to use quadruple precision, on the fly, when numerical instabilities are detected. We have observed that the numerical integration of the virtual corrections, in particular for the EW case, shows numerical instabilities. The solution to this problem used by the `LoopInts` library is described as follows. When using the MR method, the small mass regulators are neglected as much as possible for IR-safe one-loop integrals. This has to be consistently done from the top level of tensor coefficients to the bottom level of scalar integrals to ensure a regular behavior of the tensor coefficients in the limit of vanishing Gram determinant ($\det(2p_ip_j)$ with p_i being external momenta). After this step, the Gram determinant is checked for N-point tensor coefficients ($N = 3, 4$), and if it is small enough, i.e.

$$\frac{\det(2p_ip_j)}{(2p^2_{\text{max}})^{N-1}} < 10^{-3}, \quad i,j = 1,\ldots,N-1, \tag{2.12}$$

where p^2_{max} is the maximum external mass of a triangle or box diagram, then all those tensor coefficients are calculated with quadruple precision. Otherwise double precision is used. The `C++` library detects numerical instabilities based on the condition number of the Gram matrix supplemented by an additional evaluation using a different floating point rounding mode in cases of doubt. If the result is numerically unstable the loop integrals in question are evaluated in quadruple precision using the `QD` library [26]. For five-point tensor coefficients, both libraries use the method of ref. [6] to avoid the small Gram determinant problem. Moreover, the real corrections have been checked by comparing the results of the dipole-subtraction method with those of the phase-space slicing method [27].

2.3 Hadronic cross section

The LO hadronic cross section is given by

$$\sigma_{\text{LO}} = \int \mathrm{d}x_1\mathrm{d}x_2[\bar{q}_{\text{LO}}(x_1,\mu_F)q_{\text{LO}}(x_2,\mu_F)\hat{\sigma}^{\bar{q}q}_{LO}(\alpha^3) + (1\leftrightarrow 2)], \tag{2.13}$$

JHEP12(2013)096

where q and $\bar{q}$ are LO parton distribution functions of the light quarks in the proton at momentum fraction x and factorization scale μ_F. The bottom-quark contribution $\sigma_{\bar{b}b}$ is calculated in the same way. The top-quark contribution is neglected and the photon contribution reads

$$\sigma_{\gamma\gamma} = \int \mathrm{d}x_1 \mathrm{d}x_2 [\gamma(x_1,\mu_F)\gamma(x_2,\mu_F)\hat{\sigma}_{\gamma\gamma}(\alpha^3)], \tag{2.14}$$

where the photon PDF is given by the code MRSTQED2004 [28] as discussed below.

The NLO hadronic cross section is defined as follows:

$$\sigma_{\mathrm{NLO}} = \sigma^{\bar{q}q}_{\mathrm{QCD}}(\alpha^3,\alpha^3\alpha_s) + \Delta\sigma^{\bar{q}q}_{\mathrm{EW}}(\alpha^4) + \sigma_{\bar{b}b}(\alpha^3) + \sigma_{\gamma\gamma}(\alpha^3), \tag{2.15}$$

where the first term including the tree-level and NLO QCD corrections is calculated with NLO PDFs, the second term is the NLO EW correction.

We now discuss the issue of PDFs. Ideally, we would choose a NLO PDF set including QCD and EW corrections for the NLO results. However, there exists at the present no PDF set with NLO EW corrections. The leading EW contribution is included in the MRSTQED2004 set, and very recently also in the NNPDF set [29]. In our case, since the $\bar{q}q$ contribution is dominant we will use the MSTW2008 PDF set [30] everywhere for initial quarks. This set includes only QCD corrections. The photon PDF is needed for the LO $\gamma\gamma$ and the EW real corrections with photon in the initial state. For these contributions, we get the photon PDF from the MRSTQED2004 set. For NLO QCD corrections, since the PDFs are defined in the $\overline{\mathrm{MS}}$ factorization scheme the one-loop calculation in section 2.1 is also done in this scheme. For NLO EW corrections, i.e. the second term in eq. (2.15), we use the LO PDF set for all the quarks and the photon. The calculation is done assuming the DIS factorization scheme. We can also take the $\overline{\mathrm{MS}}$ scheme as in the QCD case, but there is really no justification for either choice since the quark PDFs include no EW corrections. We choose the DIS scheme because it is usually used for NLO EW corrections (see e.g. [31]). Accordingly, the PDF counterterms which appear in the real corrections are defined as follows, here q stands for both quarks and anti-quarks, in mass regularization (MR)

$$\begin{aligned}
\delta^{\mathrm{MR}} q(x,\mu_{\mathrm{F}}^2) = & -\frac{\alpha_s C_F}{2\pi}\int_x^1 \frac{dz}{z} q\left(\frac{x}{z},\mu_F^2\right)\left\{\ln\left(\frac{\mu_F^2}{m_q^2}\right)[P_{qq}(z)]_+ + P_{qq}^{\mathrm{reg}}(z) + C_{qq}^{\overline{\mathrm{MS}}}(z)\right\} \\
& -\frac{\alpha Q_q^2}{2\pi}\int_x^1 \frac{dz}{z} q\left(\frac{x}{z},\mu_F^2\right)\left\{\ln\left(\frac{\mu_F^2}{m_q^2}\right)[P_{qq}(z)]_+ + P_{qq}^{\mathrm{reg}}(z) + C_{qq}^{\mathrm{DIS}}(z)\right\} \\
& -\frac{\alpha_s T_F}{2\pi}\int_x^1 \frac{dz}{z} g\left(\frac{x}{z},\mu_F^2\right)\left[\ln\left(\frac{\mu_F^2}{m_q^2}\right)P_{gq} + C_{gq}^{\overline{\mathrm{MS}}}(z)\right] \\
& -\frac{3\alpha Q_q^2}{2\pi}\int_x^1 \frac{dz}{z} \gamma\left(\frac{x}{z},\mu_F^2\right)\left[\ln\left(\frac{\mu_F^2}{m_q^2}\right)P_{\gamma q} + C_{\gamma q}^{\mathrm{DIS}}(z)\right],
\end{aligned} \tag{2.16}$$

$$\delta^{\mathrm{MR}}\gamma(x,\mu_{\mathrm{F}}^2) = -\frac{\alpha}{2\pi}\sum_q Q_q^2 \int_x^1 \frac{dz}{z} q\left(\frac{x}{z},\mu_F^2\right)\left[\ln\left(\frac{\mu_F^2}{m_q^2}\right)P_{q\gamma} + P_{q\gamma}^{\mathrm{reg}}(z) + C_{q\gamma}^{\mathrm{DIS}}(z)\right] \tag{2.17}$$

with $C_F = 4/3$, $T_F = 1/2$ and (see e.g. [32])

$$\begin{aligned}
P_{qq}^{\mathrm{reg}}(z) &= -[P_{qq}(z)(2\ln(1-z)+1)]_+, \\
P_{q\gamma}^{\mathrm{reg}}(z) &= -P_{q\gamma}(z)(2\ln z + 1).
\end{aligned} \tag{2.18}$$

JHEP12(2013)096

The corresponding DR counterterms, $\delta^{\rm DR}q(x,\mu_{\rm F}^2)$ and $\delta^{\rm DR}\gamma(x,\mu_{\rm F}^2)$, are obtained from eqs. (2.16), (2.17) using the following rules

$$\log(m_q^2) \to \frac{1}{\epsilon} - \gamma_{\rm E} + \log(4\pi\mu^2), \quad P_{qq}^{\rm reg}(z) \to 0, \quad P_{q\gamma}^{\rm reg}(z) \to 0, \tag{2.19}$$

where we have used $D = 4 - 2\epsilon$, $\gamma_{\rm E}$ is Euler's constant and μ is the usual mass-dimension parameter in DR. This replacement rule agrees with the standard definition in [13] for DR. Moreover, we have explicitly checked eq. (2.19) by verifying numerically for various processes [33] that the results obtained using MR agree with the DR ones. The gluon PDF does not occur at LO in our calculation, therefore its counterterm does not appear at NLO.

The splitting functions are given by

$$P_{qq}(z) = \frac{1+z^2}{1-z}, \quad P_{gq}(z) = P_{\gamma q}(z) = z^2 + (1-z)^2, \quad P_{q\gamma}(z) = \frac{1+(1-z)^2}{z}, \tag{2.20}$$

and the $[\ldots]_+$ prescription is understood in the usual way,

$$\int_0^1 dz [g(z)]_+ f(z) = \int_0^1 dz\, g(z)[f(z) - f(1)]. \tag{2.21}$$

The factorization schemes are specified by [13]

$$\begin{aligned} C_{qq}^{\overline{\rm MS}}(z) &= C_{gq}^{\overline{\rm MS}}(z) = 0, \\ C_{qq}^{\rm DIS}(z) &= \left[P_{qq}(z)\left(\ln(\frac{1-z}{z}) - \frac{3}{4}\right) + \frac{9+5z}{4}\right]_+, \\ C_{\gamma q}^{\rm DIS}(z) &= P_{\gamma q}\ln(\frac{1-z}{z}) - 8z^2 + 8z - 1, \; C_{q\gamma}^{\rm DIS}(z) = -C_{qq}^{\rm DIS}(z). \end{aligned} \tag{2.22}$$

3 Numerical results

We use the following set of input parameters [1, 2, 34],

$$\begin{aligned} G_\mu &= 1.16637 \times 10^{-5}\,{\rm GeV}^{-2}, \quad \alpha(0) = 1/137.035999679, \quad \alpha_s(M_Z) = 0.12018, \\ M_W &= 80.385\,{\rm GeV}, \quad M_Z = 91.1876\,{\rm GeV}, \quad m_t = 173.5\,{\rm GeV}, \quad M_H = 125\,{\rm GeV}, \end{aligned} \tag{3.1}$$

where the strong coupling constant $\alpha_s(M_Z)$ occurs only in the NLO QCD corrections and is determined from the NLO MSTW2008 PDF set with five quark flavors as discussed in section 2.3. The Cabibbo-Kobayashi-Maskawa matrix is set to be diagonal. The masses of the light quarks, i.e. all but the top mass, are approximated as zero. This is justified because our results are insensitive to those small masses. As argued in section 2.2, the NLO EW corrections are proportional to $\alpha_{G_\mu}^3\alpha(0)$ while the $\gamma\gamma$ contribution is of $\mathcal{O}(\alpha_{G_\mu}\alpha(0)^2)$. In the following we present the results for the LHC at 14 TeV.

3.1 Total cross section

The NLO results depend on the renormalization scale μ_R and factorization scale μ_F, which are arbitrary parameters. μ_R occurs via the strong coupling constant and explicitly in the

JHEP12(2013)096

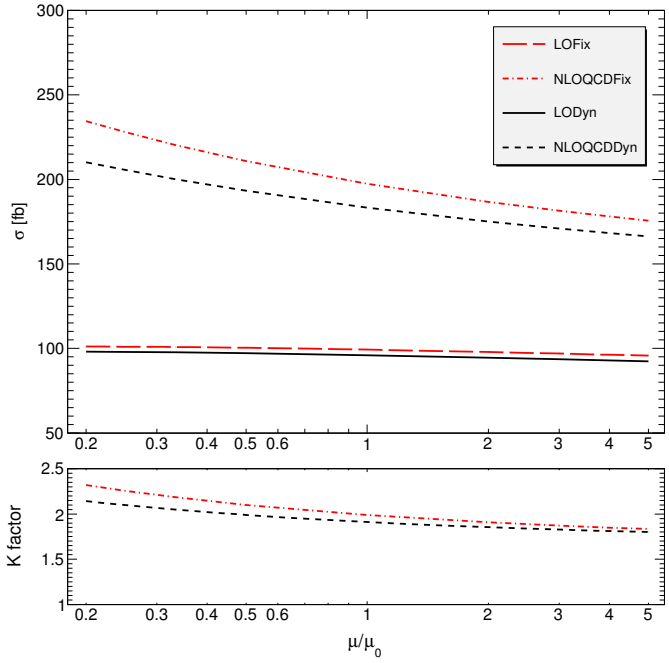

Figure 4. Total cross sections and K factor (defined in the text) as functions of the scale $\mu = \mu_F = \mu_R$.

virtual QCD amplitude. The virtual EW amplitude does not introduce any μ_R dependence since it is calculated using the OS renormalization scheme. μ_F occurs via the PDFs and explicitly in the collinear counterterms. The EW factorization scale dependence is much smaller than the QCD one, hence can be neglected. The scales μ_F and μ_R are hereafter meant to be of QCD origin. For simplicity they will be set equal and be referred to as the scale μ.

In figure 4 we show the LO and the NLO QCD total cross sections as functions of μ varied around the center scale μ_0 for two cases: a fixed scale with $\mu_0 = 2M_W + M_Z$ and a dynamic scale $\mu_0 = M_{WWZ}$, the invariant mass of triple-boson system. The K factor, defined as the ratio of the NLO to the LO results, is in the lower panel. We observe that the NLO QCD correction is about 100% and the scale uncertainty does not give a good estimate of the higher-order contribution. The fixed-scale results are similar to the dynamic ones for both the total cross section and the distributions we have studied. The small μ dependence of the LO total cross section can be explained as follows. The M_{WWZ} distribution is maximal near the threshold, at $M^{\max}_{WWZ} \approx 400\,\text{GeV}$. This corresponds to $\sqrt{x_1 x_2} = M^{\max}_{WWZ}/\sqrt{s} = 0.03$ for $\sqrt{s} = 14\,\text{TeV}$. The rapidity WWZ distribution is maximal at $y^{\max}_{WWZ} = 0$, which means $x_1 = x_2$. Thus, the main contribution to the total cross section comes from the region $x_1 = x_2 = 0.03$ where the PDFs have a small factorization scale dependence. The same argument holds for the NLO results, hence the scale dependence at NLO is given mainly by the renormalization scale. Some values of the total cross section corresponding to figure 4 are given in table 1.

The NLO QCD corrections have been calculated by two groups [3, 35] and [4]. A comparison was done in ref. [35] and the NLO QCD result of ref. [3] was about 0.5% higher

JHEP12(2013)096

	Fixed scale		Dynamic scale	
μ	LO	NLO QCD	LO	NLO QCD
$\mu_0/4$	101.02(2)	227.94(4)	97.98(2)	205.57(4)
$\mu_0/2$	100.39(2)	210.76(4)	97.11(2)	193.25(3)
μ_0	99.29(2)	197.41(4)	95.91(2)	183.31(3)
$2\mu_0$	97.87(2)	186.70(3)	94.48(2)	175.11(3)
$4\mu_0$	96.25(2)	178.01(3)	92.91(2)	168.26(3)

Table 1. Total cross section (in fb) shown in figure 4 as function of the scale $\mu = \mu_F = \mu_R$.

		Fixed scale		Dynamic scale	
		$\sigma[fb]$	$\delta[\%]$	$\sigma[fb]$	$\delta[\%]$
LO		99.29(2)	...	95.91(2)	...
$\bar{b}b$		2.4173	2.4	2.6915	2.8
$\gamma\gamma$		4.852	4.9	5.559	5.8
$\Delta_{\rm QCD}$	$q\bar{q}$	48.83(3)	49.2	53.33(3)	55.6
	$qg, \bar{q}g$	49.29(1)	49.6	34.07(1)	35.5
$\Delta_{\rm EW}$	$q\bar{q}$	-8.74(1)	-8.8	-8.05(1)	-8.4
	$q\gamma, \bar{q}\gamma$	6.81(1)	6.8	5.854(9)	6.1
$\Delta_{\rm NLO}$		103.46(4)	104.2	93.46(4)	97.4

Table 2. Total cross section in fb for $pp \to W^+W^-Z$ including the QCD NLO and EW NLO corrections at $\sqrt{s} = 14\,\text{TeV}$ for fixed scale $\mu_F = \mu_R = 2M_W + M_Z$ and dynamic scale $\mu_F = \mu_R = M_{WWZ}$. The numbers in brackets show the integration uncertainty in the last digit if they are significant.

than the one of ref. [4]. The statistical error was also about 0.5%. However, our result is about 1.5% smaller than the one of ref. [3]. By doing a tuned comparison at the amplitude level with our calculation, it was discovered that there was a bug in the calculation of the virtual amplitude in ref. [3].[1] After correcting the code, the new result of ref. [3] agrees very well with ours, at the level of 12 digits at the amplitude level with double precision. The total cross sections agree at the per mille level and within the statistical error.

We now include the NLO EW corrections as well the LO $\bar{b}b$ and $\gamma\gamma$ contributions. They are shown in table 2 for the fixed and dynamic scale choices. In this table and the following discussions the relative corrections are normalized to $\sigma_{\rm LO}$ defined in eq. (2.13). The correction coming from $\bar{b}b$ initial state is less than 3% while the $\gamma\gamma$ one is about two times lager. For the dynamic scale choice, if $\mu_F = M_{WWZ}$ is outside the allowed energy range of the MRSTQED2004 code, namely $\mu_F^2 > 10^7\,\text{GeV}^2$, then the photon PDF is set to zero. The impact of this cut should be very small since the contribution from that phase-space region is suppressed. The study of the EW correction to $\gamma\gamma \to W^+W^-$ in ref. [33] gives, for the total cross section, a per mille correction on top of the LO $\gamma\gamma$ contribution.

[1] The calculation of ref. [3] was implemented in the `VBFNLO` program [36, 37]. We thank Michael Rauch for this useful comparison.

JHEP12(2013)096

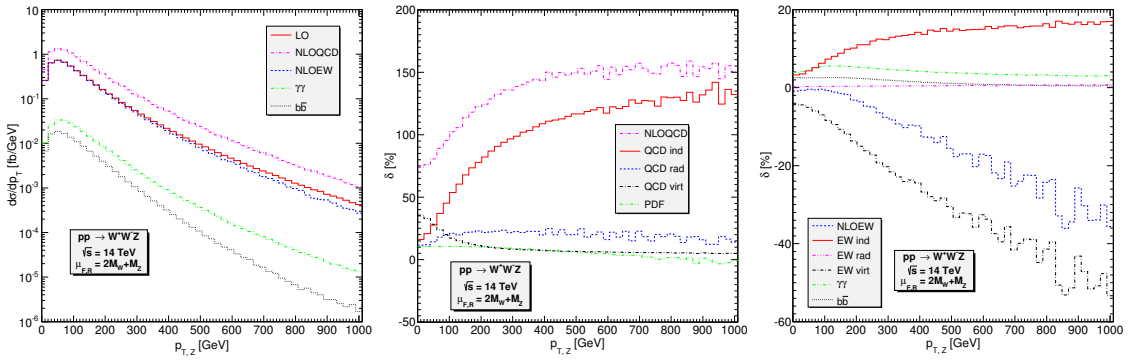

Figure 5. Z transverse momentum distributions of $pp \to W^+W^-Z$ cross section (left), of the NLO QCD corrections (middle) and of the NLO EW corrections (right). The LO distribution is plotted only in the left panel. The corrections are defined relative to the LO distribution.

We also expect the same effect for $\gamma\gamma \to W^+W^-Z$, hence NLO EW corrections to this subprocess are neglected.

In table 2 and also in section 3.2 we also show several subcorrections as defined in section 2.1 for the QCD case and in section 2.2 for the EW case. For the QCD correction, we have: the PDF correction coming from the difference between the NLO and LO PDFs, the gluon-radiated correction, the gluon-quark induced correction and the virtual correction, as defined in section 2.1. The PDF, virtual and gluon-radiated corrections are combined in the entry $q\bar{q}$ in table 2, but they are separately shown in section 3.2. Similarly, the EW correction is also separated into the photon-radiated, photon-quark induced and virtual corrections. The PDF correction vanishes because the LO PDFs are used for the EW corrections. The virtual and photon-radiated corrections are combined in the entry $q\bar{q}$ in table 2, but they are separately shown in section 3.2. In the case of the QCD corrections the $q\bar{q}$ and gluon-quark induced contributions are of the same order of magnitude and have the same positive sign. In contrast, the two contributions in the EW correction have opposite signs. This makes the total NLO EW correction about -2%.

We close this subsection with some comments on the single-top contribution. If one considers the NLO QCD corrections to $\bar{b}b \to W^+W^-Z$ channel, there is a large contribution from the gluon-quark induced process $bg \to W^+W^-Zb$ due to the mechanism $bg \to W^-Zt(t \to W^+b)$ with an intermediate on-shell top quark. This large WZt production mode, being a part of the singe-top background, should be excluded and our main concern is the interference between this mechanism and the genuine WWZ channel without the on-shell top quark. As in the W^+W^- case [33], this interference effect is expected to be negligible. We therefore neglect the NLO QCD corrections to $\bar{b}b \to W^+W^-Z$ subprocess.

3.2 Distributions

We do not observe any important difference between the fixed scale and dynamic scale results for various distributions. We therefore show only some representative distributions with the fixed scale choice.

JHEP12(2013)096

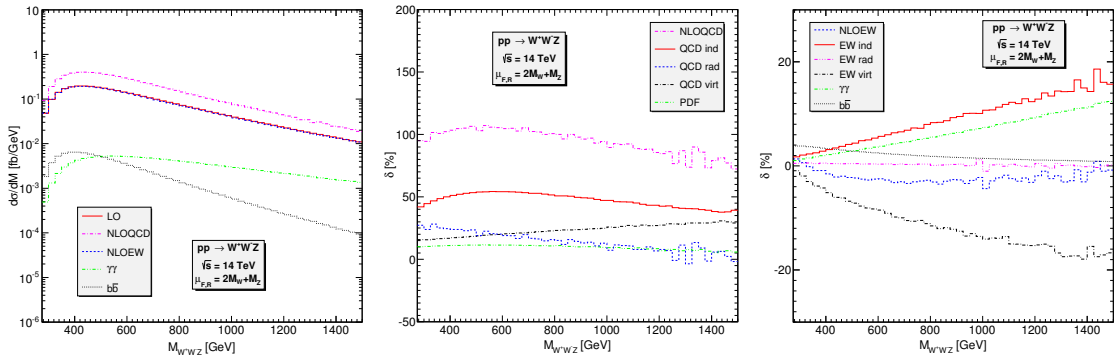

Figure 6. Same as figure 5 but for the invariant mass of the WWZ system.

We present the differential cross sections for the LO contribution as well as the $b\bar{b}$, $\gamma\gamma$, NLO QCD and NLO EW corrections. The relative corrections compared to the LO distributions are also shown. Furthermore, the various QCD and EW subcorrections defined in section 3.1 are displayed.

The Z transverse momentum distribution is shown in figure 5. From left to right we find the differential cross sections, the NLO QCD and NLO EW corrections. The differential cross sections show a maximum at about $p_T = 50\,\text{GeV}$ and decrease rapidly with p_T. The $b\bar{b}$ and $\gamma\gamma$ contributions are about 1 to 2 orders of magnitude smaller than the $q\bar{q}$ contribution in the whole p_T range. The NLO QCD correction ($b\bar{b}$ channel excluded) increases rapidly at low p_T range and is nearly constant for $p_T > 400\,\text{GeV}$. The dominant contribution comes from the gluon-quark induced subprocesses. The remaining contributions are less than 30%. The reason for this large gluon-quark induced correction is that this is a new process with large gluon PDF opening up at NLO. At large p_T, the dominant contribution comes from the mechanism where first the reaction $ug \to Zu$ with a hard Z balanced by a hard quark occurs. Then, on top of this, two soft gauge bosons W^+ and W^- are radiated. These soft boson radiations introduce two double logarithms $\alpha^2 \log^4(p_{T,Z}^2/M_W^2)$. At LO, the hard Z recoils against one W, hence there is only one double logarithm $\alpha \log^2(p_{T,Z}^2/M_W^2)$ from the soft radiation of the other W. This phenomenon is also observed in $pp \to VV$ with $V = W^\pm, Z$ [33]. While the gluon-quark induced correction can reach 900% for the W^-Z channel at $p_T = 700\,\text{GeV}$ [33], we get here about 120% for W^+W^-Z production, which is comparable to the correction in the ZZ case [33]. For the $W^\pm$ transverse momentum distributions, the correction is smaller. Moreover, we observe that the virtual correction rises up in the limit $p_T \to 0$.

For the NLO EW corrections, the virtual part is negative in the whole p_T range and behaves like $\alpha \log^2(M_V^2/p_T^2)$, reaching about -50% at $p_T = 1\,\text{TeV}$. This is the well-known Sudakov double logarithm arising from the exchange of a virtual massive gauge boson in the loops. For the photon-quark induced correction, the above picture of the gluon-quark induced correction holds. There are, however, some important differences. Naively, one would expect that this correction must be very small because of the EW coupling and small photon PDF, as it is the case for the $pp \to ZZ$ process [33]. But, as in the case of photon-quark induced corrections to $W^\pm Z$ and W^+W^- production [33], there is a new

JHEP12(2013)096

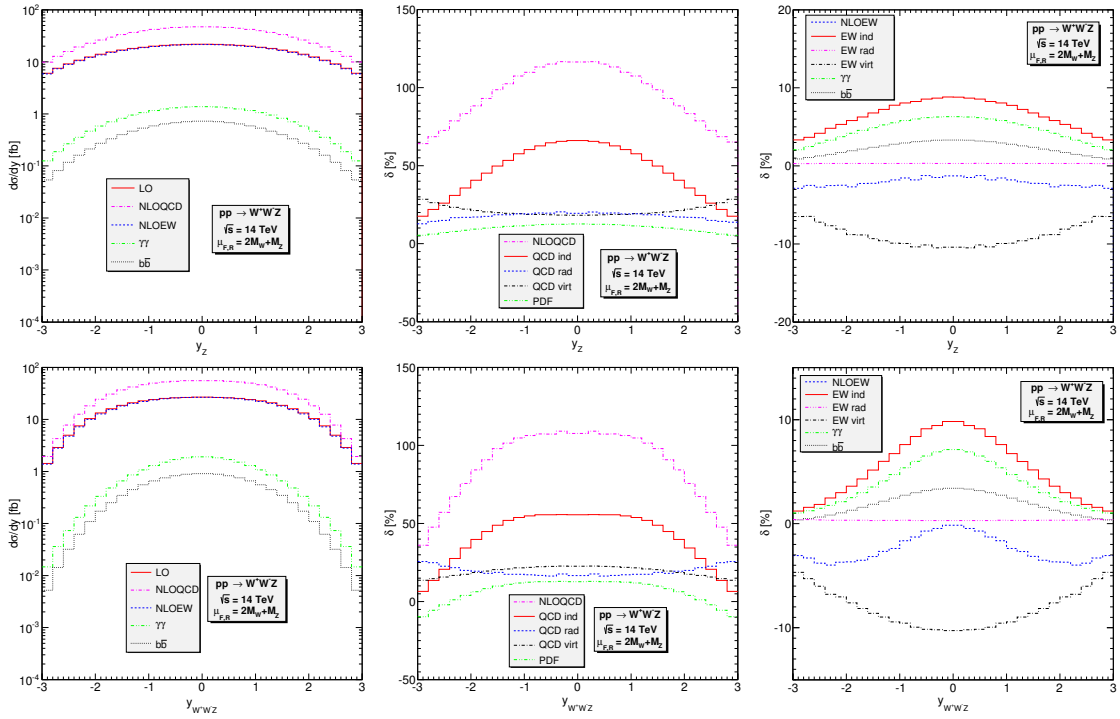

Figure 7. Same as figure 5 but for the rapidity of the Z (first row) and of the WWZ system (second row).

enhancement mechanism in the hard $2 \to 2$ amplitude due to the t-channel exchange of a W gauge boson as shown in the first diagram in figure 3(b). The hard processes are $qg \to qZ$ for the gluon-quark induced case, while it can be $uW^- \to dZ$ for the photon-quark induced channels. By a simple dimensional analysis, we get at partonic level and from the t-channel diagrams $|\mathcal{A}_{uW^-\to dZ}|^2/|\mathcal{A}_{ug\to uZ}|^2 \propto E_u^2/q^2$ with $q^2 \approx -2E_u^2(1-\cos\theta)$ being the momentum-transfer square. This enhancement factor for moderate q^2 and some possible additional enhancement from the couplings can lead to a significant enhancement to compensate for the smallness of the photon PDF. At the end we observe nearly +20% photon-quark induced correction at $p_{T,Z} = 1\,\text{TeV}$, canceling part of the Sudakov virtual correction.

In figure 6, we present the invariant mass distribution of the W^+W^-Z system. For QCD corrections, all contributions are positive and the maximal total correction is slightly above 100% at $M_{WWZ} = 500\,\text{GeV}$. Turning to the EW correction plot, we see that the $b\bar{b}$ contribution is important at low energy while the $\gamma\gamma$ channel is very important at large invariant mass. The full NLO EW correction ($\gamma\gamma$ and $b\bar{b}$ both excluded) is very small (less than 4%) in the whole range. This is due to the cancellation between the photon-quark induced and virtual corrections as shown in the plot. The $\gamma\gamma$ correction is larger than the full EW one at large invariant mass.

We next display in figure 7 the rapidity distribution of the Z boson in the first row and of the W^+W^-Z system in the second row. One can see that both the Z boson and the W^+W^-Z system are centrally produced. In both cases, the QCD correction is dominated

JHEP12(2013)096

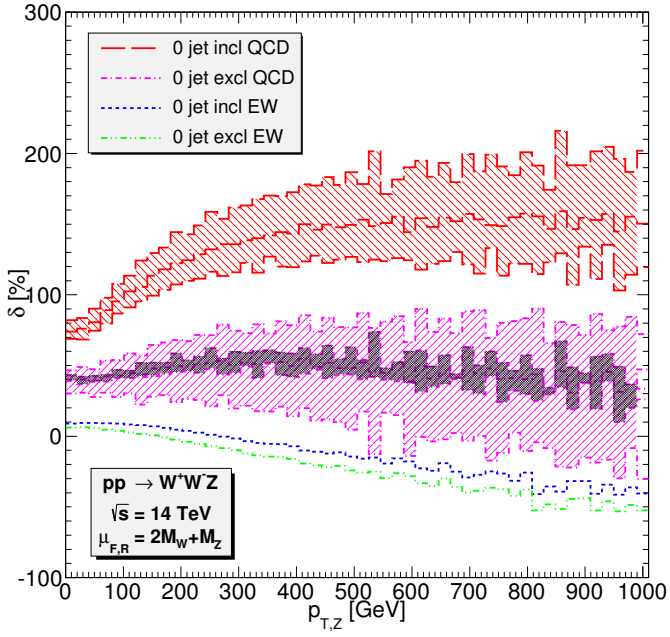

Figure 8. NLO QCD and EW corrections to the Z transverse momentum distribution for inclusive events without jet cuts and also for exclusive events with a dynamic jet veto defined in the text. The bands describe $\mu_0/2 \leq \mu_F = \mu_R \leq 2\mu_0$ with $\mu_0 = 2M_W + M_Z$ variations of the NLO QCD corrections. The LO result is calculated at the central scale everywhere. The band at the top is for the inclusive distribution. The two other bands are for the exclusive distribution. Their definitions are given in the text.

by the gluon-quark induced contribution and maximal in the central region. For the EW correction plot, we again see the importance of the $\gamma\gamma$ channel and the cancellation between the photon-quark induced and virtual corrections. In both cases, the full EW correction is negative and its magnitude is always less than 5%.

From the above phase-space dependence study, we see that the NLO QCD correction mainly due to the $2 \to 4$ gluon-quark induced channels is very large at high p_T. The dominant contribution comes from the region where the quark transverse momentum is large. It is therefore attractive to think of imposing a jet veto to reduce this large QCD contribution, as done for example in refs. [38, 39]. One should be very careful in doing so because using a jet veto increases theoretical uncertainty due to missing large higher-order corrections [40, 41]. In this sense, the cross section with jet veto is less perturbative than the inclusive cross section. This view is supported in figure 8. Here we apply a dynamic jet veto: for the exclusive zero-jet distribution, we veto events with $p_{\mathrm{T,jet}} > p_{\mathrm{veto}}$, with

$$p_{\mathrm{veto}} = \frac{1}{2}\max(M_{\mathrm{T},W^+}, M_{\mathrm{T},W^-}, M_{\mathrm{T},Z}), \tag{3.2}$$

where $M_{\mathrm{T},V} = (p^2_{\mathrm{T},V} + M^2_V)^{1/2}$ is the transverse mass. We have tried a fixed jet veto with $p_{\mathrm{veto}} = 25\,\mathrm{GeV}$ and found that it over subtracts the NLO QCD correction, leading to large negative QCD correction at high $p_{T,Z}$. With the dynamic jet veto, we found that

JHEP12(2013)096

more than half of the QCD correction is removed. However, the uncertainty band on the exclusive zero-jet distribution is larger than the band on the inclusive zero-jet distribution. The reason is the following. We have

$$d\sigma_{0\text{j,inc}} = d\sigma_{0\text{j,exc}} + d\sigma_{1\text{j,inc}}. \tag{3.3}$$

The inclusive zero-jet distribution $d\sigma_{0\text{j,inc}}$ is independent of p_{veto}, while both the exclusive zero-jet $d\sigma_{0\text{j,exc}}$ and inclusive one-jet $d\sigma_{1\text{j,inc}}$ distributions depend on $\log(p_{\text{veto}}/p_{T,Z})$. The two terms in the right-hand side of eq. (3.3) are therefore not independent. Thus, as argued in ref. [40], it is suitable to consider $d\sigma_{0\text{j,inc}}$ and $d\sigma_{1\text{j,inc}}$ as independent observables and calculate $d\sigma_{0\text{j,exc}}$ from them. This means that the scale uncertainty of the exclusive zero-jet distribution is calculated as

$$\Delta^2_{0\text{j,exc}} = \Delta^2_{0\text{j,inc}} + \Delta^2_{1\text{j,inc}}. \tag{3.4}$$

This explains the large uncertainty band (in pink) of the exclusive distribution. In passing, we also show the naive uncertainty band (the smallest band in black) calculated as $\Delta_{0\text{j,exc}} = \Delta_{0\text{j,inc}} - \Delta_{1\text{j,inc}}$ assuming that the two inclusive observables are anti-correlated.

In figure 8, we also show the effect of the dynamic jet veto on the EW correction. Here, for the photon-radiated contribution, the photon is treated as a jet. We observe a small effect. For the EW correction, there is no uncertainty band because the scale dependence is of QCD origin as pointed out in section 3.1.

4 Conclusions

In this paper, we have presented the first calculation of the NLO EW correction in combination with the NLO QCD correction to the W^+W^-Z production at the LHC with 14 TeV center-of-mass energy. This provides the most up-to-date prediction of the total and differential cross sections. The NLO QCD correction is large, about +100% for the total cross section. For EW correction, not only the photon-radiated but also the photon-quark induced contributions are taken into account. The latter turns out to be important and cancel part of the large Sudakov virtual correction. This leads to very small EW correction, about −2%, for the total cross section. This cancellation happens, to varying extent, also in the transverse momentum, invariant mass and rapidity distributions.

We have also discussed the use of a jet veto to reduce the large QCD correction. We found that using a dynamic jet veto is good in the sense that it allows the jet to be away from the non-perturbative regime and removes significantly the QCD correction. On other hand, it increases QCD uncertainty due to missing large higher-order corrections.

A Results at one phase-space point

In this appendix we provide results at a random phase-space point to facilitate comparisons with our results, in particular for those trying to develop automated tools. The phase-space point for the process $\bar{q}q \to W^+W^-Z$ is given in table 3. In the following we provide

JHEP12(2013)096

	E	p_x	p_y	p_z
$\bar{q}$	234.035328935400	0.0	0.0	234.035328935400
q	234.035328935400	0.0	0.0	-234.035328935400
W^+	204.344376484520	-120.509782379302	28.2759628195356	141.324938540120
W^-	133.625238535211	87.1775591913742	-28.2759628195356	-54.7220179512301
Z	130.101042851068	33.3322231879280	0.0	-86.6029205888900

Table 3. Momenta in GeV at a random phase-space point for $\bar{q}q \to W^+W^-Z$ subprocesses.

	$1/\epsilon^2$	$1/\epsilon$	finite
QCD-I	0.408180656656545	0.106650712644880	-0.418657743041666
QCD-loop	-0.408180656656539	-0.106650712644797	1.63036547637921
QCD-virt	$5.307828480419084\times10^{-15}$	$8.387679573995589\times10^{-14}$	1.21170773333755

Table 4. QCD interference amplitudes $2\mathrm{Re}(\mathcal{A}_{\mathrm{NLO}}\mathcal{A}^*_{\mathrm{LO}})$ for terms in eq. (2.6) for $\bar{u}u \to W^+W^-Z$ subprocess.

	$1/\epsilon^2$	$1/\epsilon$	finite
QCD-I	5.25548706505201	1.37317002078168	-5.39038368760993
QCD-loop	-5.25548706505202	-1.37317002078186	19.8522399631644
QCD-virt	$-3.145379840248346\times10^{-15}$	$-1.813835707876546\times10^{-13}$	14.4618562755545

Table 5. QCD interference amplitudes $2\mathrm{Re}(\mathcal{A}_{\mathrm{NLO}}\mathcal{A}^*_{\mathrm{LO}})$ for terms in eq. (2.6) for $\bar{d}d \to W^+W^-Z$ subprocess.

the squared amplitude with the averaged factor over helicities and colors. We also set $\alpha = \alpha_s = 1$ for simplicity. At tree level, we have

$$\begin{aligned} \overline{|\mathcal{A}^{\bar{u}u}_{\mathrm{LO}}|}^2 &= 0.961753014217244, \\ \overline{|\mathcal{A}^{\bar{d}d}_{\mathrm{LO}}|}^2 &= 12.3829496659527. \end{aligned} \tag{A.1}$$

The interference amplitudes $2\mathrm{Re}(\mathcal{A}_{\mathrm{NLO}}\mathcal{A}^*_{\mathrm{LO}})$, for the virtual QCD corrections defined in eq. (2.6), are given in table 4 and table 5. Here we use the following convention for one-loop integrals, with $D = 4 - 2\epsilon$,

$$T_0 = \frac{\mu^{2\epsilon}\Gamma(1-\epsilon)}{i\pi^{2-\epsilon}} \int d^D q \frac{1}{(q^2 - m_1^2 + i0)\cdots}. \tag{A.2}$$

This amounts to dropping a factor $(4\pi)^\epsilon/\Gamma(1-\epsilon)$ both in the virtual corrections and the I-operator. Moreover, the dimensional regularization method [12, 23] with $\mu_F = \mu_R = 2M_W + M_Z$ is used. For the dimensional reduction scheme, the I-operator and loop amplitudes are different, but their sum must be the same [42]. The finite part of the virtual QCD correction is independent of μ_F and μ_R.

For EW corrections, we use mass regularization and the results are given in table 6. Note that, as written in section 2.2, the I-operator contribution is now defined as the endpoint contribution in ref. [21]. The light fermion mass regulator is $m_f = 10^{-4}\,\mathrm{GeV}$

JHEP12(2013)096

	$\bar{u}u \to W^+W^-Z$	$\bar{d}d \to W^+W^-Z$
EW-I	-8.09003628219715	-34.6814203416028
EW-loop	-10.5259914893826	-70.1705883597006
EW-virt	-18.6160277715797	-104.852008701303

Table 6. Interference amplitudes $2\mathrm{Re}(\mathcal{A}_{\mathrm{NLO}}\mathcal{A}^*_{\mathrm{LO}})$ for EW corrections as defined in the text.

(with $f \neq t$). We have checked that the virtual EW correction, i.e. the sum of the I-operator and loop contributions, is UV and IR finite as well as independent of m_f. If we change to $m_f = 10^{-3}(10^{-5})\,\mathrm{GeV}$ then we obtain 8(10) digit agreement using double precision.

Acknowledgments

We thank Dieter Zeppenfeld for fruitful discussions. We are grateful to Nicolas Greiner, Giovanni Ossola and Michael Rauch for comparisons at NLO QCD. This work is supported by the Deutsche Forschungsgemeinschaft via the Sonderforschungsbereich/Transregio SFB/TR-9 Computational Particle Physics.

References

[1] ATLAS collaboration, *Observation of a new particle in the search for the Standard Model Higgs boson with the ATLAS detector at the LHC*, *Phys. Lett.* **B 716** (2012) 1 [arXiv:1207.7214] [INSPIRE].

[2] CMS collaboration, *Observation of a new boson at a mass of 125 GeV with the CMS experiment at the LHC*, *Phys. Lett.* **B 716** (2012) 30 [arXiv:1207.7235] [INSPIRE].

[3] V. Hankele and D. Zeppenfeld, *QCD corrections to hadronic WWZ production with leptonic decays*, *Phys. Lett.* **B 661** (2008) 103 [arXiv:0712.3544] [INSPIRE].

[4] T. Binoth, G. Ossola, C. Papadopoulos and R. Pittau, *NLO QCD corrections to tri-boson production*, *JHEP* **06** (2008) 082 [arXiv:0804.0350] [INSPIRE].

[5] G. Passarino and M. Veltman, *One Loop Corrections for e^+e^- Annihilation Into $\mu^+\mu^-$ in the Weinberg Model*, *Nucl. Phys.* **B 160** (1979) 151 [INSPIRE].

[6] A. Denner and S. Dittmaier, *Reduction schemes for one-loop tensor integrals*, *Nucl. Phys.* **B 734** (2006) 62 [hep-ph/0509141] [INSPIRE].

[7] T. Binoth, J.P. Guillet, G. Heinrich, E. Pilon and C. Schubert, *An Algebraic/numerical formalism for one-loop multi-leg amplitudes*, *JHEP* **10** (2005) 015 [hep-ph/0504267] [INSPIRE].

[8] G. 't Hooft and M. Veltman, *Scalar One Loop Integrals*, *Nucl. Phys.* **B 153** (1979) 365 [INSPIRE].

[9] S. Dittmaier, *Separation of soft and collinear singularities from one loop N point integrals*, *Nucl. Phys.* **B 675** (2003) 447 [hep-ph/0308246] [INSPIRE].

JHEP12(2013)096

[10] D.T. Nhung and L.D. Ninh, *D0C : A code to calculate scalar one-loop four-point integrals with complex masses*, *Comput. Phys. Commun.* **180** (2009) 2258 [arXiv:0902.0325] [INSPIRE].

[11] A. Denner and S. Dittmaier, *Scalar one-loop 4-point integrals*, *Nucl. Phys.* **B 844** (2011) 199 [arXiv:1005.2076] [INSPIRE].

[12] G. 't Hooft and M. Veltman, *Regularization and Renormalization of Gauge Fields*, *Nucl. Phys.* **B 44** (1972) 189 [INSPIRE].

[13] S. Catani and M. Seymour, *A General algorithm for calculating jet cross-sections in NLO QCD*, *Nucl. Phys.* **B 485** (1997) 291 [*Erratum ibid.* **B 510** (1998) 503-504] [hep-ph/9605323] [INSPIRE].

[14] K. Aoki, Z. Hioki, M. Konuma, R. Kawabe and T. Muta, *Electroweak Theory. Framework of On-Shell Renormalization and Study of Higher Order Effects*, *Prog. Theor. Phys. Suppl.* **73** (1982) 1 [INSPIRE].

[15] A. Denner, *Techniques for calculation of electroweak radiative corrections at the one loop level and results for W physics at LEP-200*, *Fortsch. Phys.* **41** (1993) 307 [arXiv:0709.1075] [INSPIRE].

[16] G. Bélanger, F. Boudjema, J. Fujimoto, T. Ishikawa, T. Kaneko et al., *Automatic calculations in high energy physics and Grace at one-loop*, *Phys. Rept.* **430** (2006) 117 [hep-ph/0308080] [INSPIRE].

[17] A. Sirlin, *Radiative Corrections in the* $\mathrm{SU}(2)_L \times \mathrm{U}(1)$ *Theory: A Simple Renormalization Framework*, *Phys. Rev.* **D 22** (1980) 971 [INSPIRE].

[18] F. Jegerlehner, *Renormalizing the standard model*, in *Proceedings of TASI*, Boulder, CO, U.S.A., 1990, *Conf. Proc.* **C900603** (1990) 476.

[19] S. Dittmaier and . Kramer, Michael, *Electroweak radiative corrections to W boson production at hadron colliders*, *Phys. Rev.* **D 65** (2002) 073007 [hep-ph/0109062] [INSPIRE].

[20] A. Denner, S. Dittmaier, M. Roth and D. Wackeroth, *O(alpha) corrections to* $e^+e^- \to WW \to 4$ fermions$(+\gamma)$*: First numerical results from RACOON W W*, *Phys. Lett.* **B 475** (2000) 127 [hep-ph/9912261] [INSPIRE].

[21] S. Dittmaier, *A General approach to photon radiation off fermions*, *Nucl. Phys.* **B 565** (2000) 69 [hep-ph/9904440] [INSPIRE].

[22] T. Hahn, *Generating Feynman diagrams and amplitudes with FeynArts 3*, *Comput. Phys. Commun.* **140** (2001) 418 [hep-ph/0012260] [INSPIRE].

[23] T. Hahn and M. Pérez-Victoria, *Automatized one loop calculations in four-dimensions and D-dimensions*, *Comput. Phys. Commun.* **118** (1999) 153 [hep-ph/9807565] [INSPIRE].

[24] H. Murayama, I. Watanabe and K. Hagiwara, *HELAS: HELicity amplitude subroutines for Feynman diagram evaluations*, *Tech. Rep.*, KEK-91-11, 1992.

[25] J. Alwall, P. Demin, S. de Visscher, R. Frederix, M. Herquet et al., *MadGraph/MadEvent v4: The New Web Generation*, *JHEP* **09** (2007) 028 [arXiv:0706.2334] [INSPIRE].

[26] D. Bailey, Y. Hida and X. Li, *QD (C++/Fortran-90 double-double and quad-double package)*, http://crd.lbl.gov/~dhbailey/mpdist/.

[27] U. Baur, S. Keller and D. Wackeroth, *Electroweak radiative corrections to W boson production in hadronic collisions*, *Phys. Rev.* **D 59** (1999) 013002 [hep-ph/9807417] [INSPIRE].

JHEP12(2013)096

[28] A. Martin, R. Roberts, W. Stirling and R. Thorne, *Parton distributions incorporating QED contributions*, *Eur. Phys. J.* **C 39** (2005) 155 [hep-ph/0411040] [INSPIRE].

[29] S. Carrazza, *Towards the determination of the photon parton distribution function constrained by LHC data*, arXiv:1307.1131 [INSPIRE].

[30] A. Martin, W. Stirling, R. Thorne and G. Watt, *Parton distributions for the LHC*, *Eur. Phys. J.* **C 63** (2009) 189 [arXiv:0901.0002] [INSPIRE].

[31] K.-P. Diener, S. Dittmaier and W. Hollik, *Electroweak higher-order effects and theoretical uncertainties in deep-inelastic neutrino scattering*, *Phys. Rev.* **D 72** (2005) 093002 [hep-ph/0509084] [INSPIRE].

[32] S. Dittmaier and M. Huber, *Radiative corrections to the neutral-current Drell-Yan process in the Standard Model and its minimal supersymmetric extension*, *JHEP* **01** (2010) 060 [arXiv:0911.2329] [INSPIRE].

[33] J. Baglio, L.D. Ninh and M.M. Weber, *Massive gauge boson pair production at the LHC: a next-to-leading order story*, *Phys. Rev.* **D 88** (2013) 113005 [arXiv:1307.4331] [INSPIRE].

[34] PARTICLE DATA GROUP collaboration, J. Beringer et al., *Review of Particle Physics (RPP)*, *Phys. Rev.* **D 86** (2012) 010001 [INSPIRE].

[35] V. Hankele, *NLO QCD corrections to tri-boson production in hadronic collisions*, Ph.D. thesis, Universität Karlsruhe, 2009.

[36] K. Arnold, M. Bahr, G. Bozzi, F. Campanario, C. Englert et al., *VBFNLO: A Parton level Monte Carlo for processes with electroweak bosons*, *Comput. Phys. Commun.* **180** (2009) 1661 [arXiv:0811.4559] [INSPIRE].

[37] K. Arnold, J. Bellm, G. Bozzi, F. Campanario, C. Englert et al., *Release Note – Vbfnlo-2.6.0*, arXiv:1207.4975 [INSPIRE].

[38] F. Campanario, V. Hankele, C. Oleari, S. Prestel and D. Zeppenfeld, *QCD corrections to charged triple vector boson production with leptonic decay*, *Phys. Rev.* **D 78** (2008) 094012 [arXiv:0809.0790] [INSPIRE].

[39] A. Denner, S. Dittmaier, T. Kasprzik and A. Muck, *Electroweak corrections to W + jet hadroproduction including leptonic W-boson decays*, *JHEP* **08** (2009) 075 [arXiv:0906.1656] [INSPIRE].

[40] I.W. Stewart and F.J. Tackmann, *Theory Uncertainties for Higgs and Other Searches Using Jet Bins*, *Phys. Rev.* **D 85** (2012) 034011 [arXiv:1107.2117] [INSPIRE].

[41] C.F. Berger, C. Marcantonini, I.W. Stewart, F.J. Tackmann and W.J. Waalewijn, *Higgs Production with a Central Jet Veto at NNLL+NNLO*, *JHEP* **04** (2011) 092 [arXiv:1012.4480] [INSPIRE].

[42] S. Catani, M. Seymour and Z. Trócsányi, *Regularization scheme independence and unitarity in QCD cross-sections*, *Phys. Rev.* **D 55** (1997) 6819 [hep-ph/9610553] [INSPIRE].

JHEP12(2013)096